




BRAIN COMMUNICATIONS

Longitudinal imaging highlights preferential basal ganglia circuit atrophy in Huntington's disease

Chin-Fu Liu,^{1,2,3} Laurent Younes,^{1,2,4}  Xiao J. Tong,⁵ Jared T. Hinkle,^{6,7} Maggie Wang,^{1,3} Sanika Phatak,^{1,3} Xin Xu,⁸ Xuan Bu,^{1,2,9} Vivian Looi,^{1,2,3} Jee Bang,¹⁰ Sarah J. Tabrizi,¹¹ Rachael I. Scahill,¹¹ Jane S. Paulsen,¹²  Nellie Georgiou-Karistianis,¹³  Andreia V. Faria,⁸ Michael I. Miller,^{1,2,3} J. Tilak Ratnanather^{1,2,3} and Christopher A. Ross^{5,6,10,14}

Huntington's disease is caused by a CAG repeat expansion in the Huntingtin gene (*HTT*), coding for polyglutamine in the Huntingtin protein, with longer CAG repeats causing earlier age of onset. The variable 'Age' \times ('CAG'—L), where 'Age' is the current age of the individual, 'CAG' is the repeat length and L is a constant (reflecting an approximation of the threshold), termed the 'CAG Age Product' (CAP) enables the consideration of many individuals with different CAG repeat expansions at the same time for analysis of any variable and graphing using the CAG Age Product score as the X axis. Structural MRI studies have showed that progressive striatal atrophy begins many years prior to the onset of diagnosable motor Huntington's disease, confirmed by longitudinal multicentre studies on three continents, including PREDICT-HD, TRACK-HD and IMAGE-HD. However, previous studies have not clarified the relationship between striatal atrophy, atrophy of other basal ganglia structures, and atrophy of other brain regions. The present study has analysed all three longitudinal datasets together using a single image segmentation algorithm and combining data from a large number of subjects across a range of CAG Age Product score. In addition, we have used a strategy of normalizing regional atrophy to atrophy of the whole brain, in order to determine which regions may undergo preferential degeneration. This made possible the detailed characterization of regional brain atrophy in relation to CAG Age Product score. There is dramatic selective atrophy of regions involved in the basal ganglia circuit—caudate, putamen, nucleus accumbens, globus pallidus and substantia nigra. Most other regions of the brain appear to have slower but steady degeneration. These results support (but certainly do not prove) the hypothesis of circuit-based spread of pathology in Huntington's disease, possibly due to spread of mutant Htt protein, though other connection-based mechanisms are possible. Therapeutic targets related to prion-like spread of pathology or other mechanisms may be suggested. In addition, they have implications for current neurosurgical therapeutic approaches, since delivery of therapeutic agents solely to the caudate and putamen may miss other structures affected early, such as nucleus accumbens and output nuclei of the striatum, the substantia nigra and the globus pallidus.

- 1 Center for Imaging Science, Johns Hopkins University, Baltimore, MD 21218, USA
- 2 Institute for Computational Medicine, Johns Hopkins University, Baltimore, MD 21218, USA
- 3 Department of Biomedical Engineering, Johns Hopkins University, Baltimore, MD 21218, USA
- 4 Department of Applied Mathematics and Statistics, Johns Hopkins University, Baltimore, MD 21218, USA
- 5 Division of Neurobiology, Department of Psychiatry, Johns Hopkins University School of Medicine, Baltimore MD 21287, USA
- 6 Department of Neuroscience, Johns Hopkins University School of Medicine, Baltimore, MD 21218, USA
- 7 Medical Scientist Training Program, Johns Hopkins University School of Medicine, Baltimore, MD 21287, USA
- 8 Division of Magnetic Resonance, Department of Radiology, Johns Hopkins University School of Medicine, Baltimore, MD 21287, USA
- 9 Huaxi MR Research Center, Department of Radiology, West China Hospital of Sichuan University, Chengdu, Sichuan 610041, China

Received April 07, 2022. Revised May 09, 2023. Accepted August 17, 2023. Advance access publication August 18, 2023

© The Author(s) 2023. Published by Oxford University Press on behalf of the Guarantors of Brain.

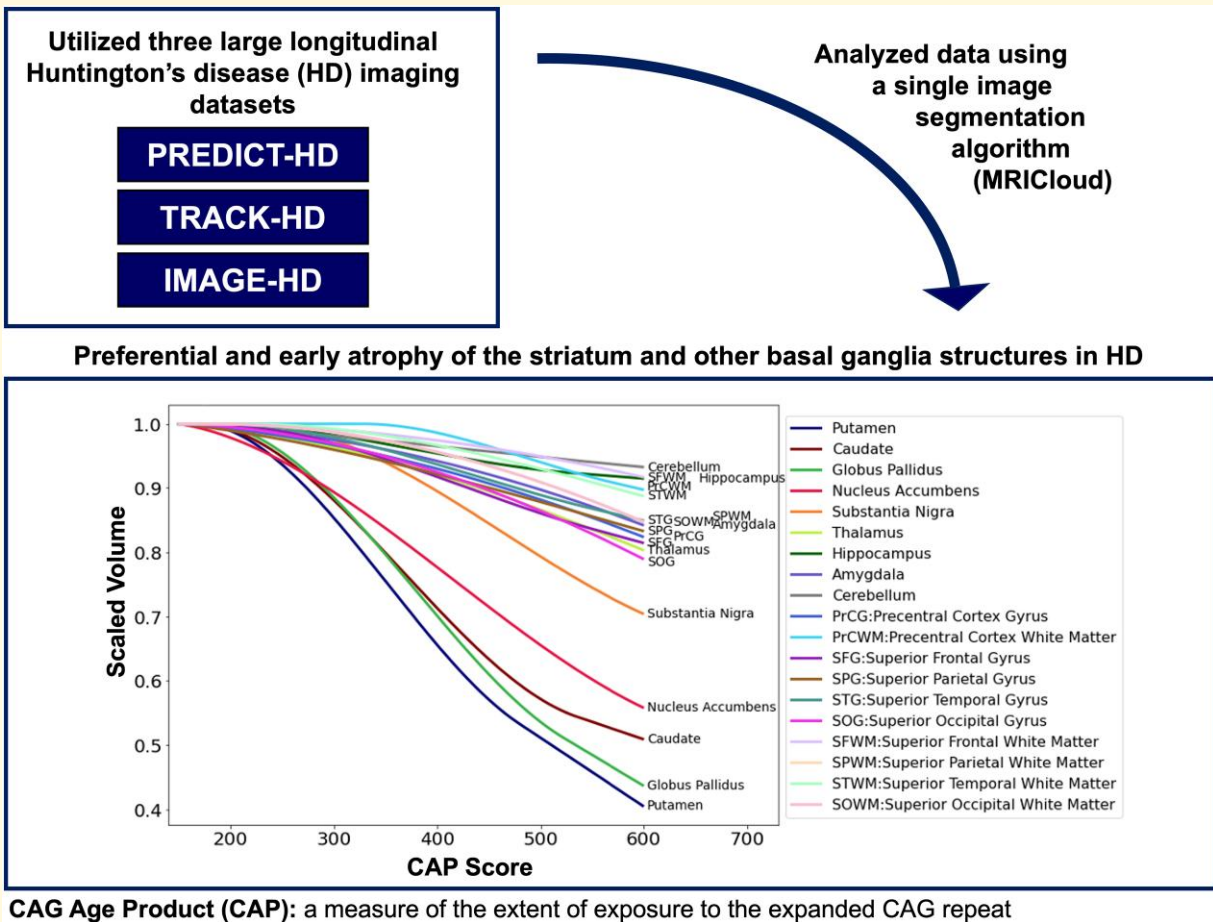
This is an Open Access article distributed under the terms of the Creative Commons Attribution License (<https://creativecommons.org/licenses/by/4.0/>), which permits unrestricted reuse, distribution, and reproduction in any medium, provided the original work is properly cited.

- 10 Division of Neurobiology, Department of Psychiatry, Department of Neurology, Johns Hopkins University School of Medicine, Baltimore, MD 21287, USA
 11 HD Research Centre, University College London Queen Square Institute of Neurology, UCL, London, UK
 12 Department of Neurology, University of Wisconsin, Madison, WI 53705, USA
 13 School of Psychological Sciences and The Turner Institute for Brain and Mental Health, Monash University, Melbourne, Victoria 3800, Australia
 14 Department of Pharmacology, Johns Hopkins University School of Medicine, Baltimore, MD 21287, USA

Correspondence to: Christopher A. Ross, MD PhD
 Division of Neurobiology, Department of Psychiatry
 600 North Wolfe Street, Baltimore, MD 21287, USA
 E-mail: caross@jh.edu

Keywords: caudate; putamen; PREDICT-HD; TRACK-HD; IMAGE-HD

Graphical Abstract



Introduction

Huntington's disease (HD) is caused by a CAG repeat expansion in the *Huntingtin* gene (*HTT*) on chromosome 4, which codes for polyglutamine in the Huntingtin protein (Htt). HD classically manifests with a triad of signs and symptoms, including motor, cognitive and behavioural features.^{1,2} Diagnosis is traditionally made based on clinician assessment of motor signs using the unified Huntington's disease rating scale (UHDRS),³

though recent developments have added cognitive changes as contributing to the diagnosis of manifest HD.⁴

The age of onset of HD is strongly influenced by the length of the CAG trinucleotide expansion within the *Huntingtin* (*HTT*) gene. Above a threshold of around 36–39 CAG, the longer the repeat length, the earlier the onset. To estimate the effects of the CAG repeat expansion over time, a variable of the form Age \times (CAG – L), where Age is the current age of the individual, CAG is the repeat length and L is a

constant (reflecting an approximation of the threshold), was first proposed by Penny *et al.*⁵ It has subsequently been termed the ‘CAG Age Product’ (CAP) score.^{1,6} It enables the consideration of many individuals with the CAG repeat expansion at the same time for analysis of any variable and graphing using the CAP score as the X axis.

Huntington’s disease has traditionally been noted for selective striatal neurodegeneration, especially early in the course. The widely used Vonsattel neuropathological staging system focuses almost entirely on striatal atrophy and cell loss.⁷ However, there has been increasing appreciation that many other regions of the brain are affected, and in a recent review, HD was described as a ‘multisystem neurodegenerative disease’.⁸

Structural MRI studies have made possible great advances in our understanding of the natural history of neurodegeneration in HD. Initial single-site studies⁹ showed that progressive striatal atrophy begins many years prior to the onset of diagnosable motor HD. This has been amply confirmed by several large studies, including the PREDICT-HD and TRACK-HD multi-centre studies, in North America and Europe, respectively, and the IMAGE-HD study in Australia.^{10–14} These studies, in addition to confirming the progressive early striatal atrophy, also called attention to atrophy in other areas such as subcortical white matter, for instance, as highlighted in the PREDICT-HD study. However, these previous studies, while very enlightening, have used different analytic methods and have emphasized slightly different results.

The present study has had the opportunity to analyse all three datasets together using a single image segmentation algorithm¹⁵ for all the scans. This has made it possible to combine data from a large number of subjects across a range of CAP scores. In addition, we have used a strategy of normalizing regional atrophy to atrophy of the whole brain, in order to determine which regions may undergo preferential degeneration. We demonstrate dramatic selective atrophy to regions involved in the basal ganglia circuit, such as caudate, putamen, nucleus accumbens, globus pallidus and substantia nigra. Most other regions of the brain appear to have slower but steady degeneration. These results have implications for the possibility of circuit-based spread of pathology in HD, suggesting pathophysiological mechanisms which may yield novel therapeutic targets. They also have implications for the design of neurosurgical approaches.

Materials and methods

Dataset

The data were obtained via CHDI from the previously published studies PREDICT-HD, TRACK-HD and IMAGE-HD.^{10–12} Each study was a longitudinal observational study including structural imaging. For PREDICT-HD, all HD subjects were premanifest at entry. TRACK-HD and IMAGE-HD had a mixture of premanifest and manifest subjects at entry. A similar approach as in this study was used in Wijeratne *et al.*,¹⁶ though

with a different imaging pipeline, different analyses and information regarding the individual studies is also summarized there.

Image preprocessing

All MRIs were automatically segmented via MRICloud,¹⁵ a public website platform for multi-contrast imaging segmentation and quantification. In MRICloud, the process of T1-WI segmentation, used for volumetric analysis, involves: (1) image pre-processing (orientation and inhomogeneity correction, skull stripping), (2) image registration to multiple atlases based on a sequence of affine transformations and the Large Deformation Diffeomorphic Mapping (LDDMM) and (3) multi-atlas labelling fusion (MALF) algorithm^{17–19} to fuse the parcellation labels of atlases for each scan. In this study, we used the atlas set ‘Adult50–90yrs_287Labels_30atlases_M2_252_V10A’, composed by 30 brain MRIs of 50–90 year-old individuals, in which 287 brain structures are defined with a multi-level hierarchical ontology.^{20,21} The performance of MRICloud pipeline, compared with human evaluators and with other state-of-the-art algorithms, was described in previous publications.^{22–24}

The original images as well as the results of the brain segmentation from MRICloud were visually inspected for quality control (QC). Images were excluded in the presence of artefacts (e.g. too much motion) or in the case of incomplete coverage (e.g. scans did not cover the top or the bottom of the brain). We excluded cases with obvious registration errors, mostly derived from the very first step of the image processing, the linear mapping to the templates. These errors are well known in imaging processing and are usually related to large rotations in the interstice axis or particularities of the field-of-view. We opted not to perform any human correction on the segmentation, as our aim is to report the results of a consistent automated process across all the images. The sample sizes and participant demographic of all three datasets, before and after QC, are summarized in Table 1 in the [supplementary material](#). After QC, the percentage of male subjects in each study is 50%, 31.8% and 47% for IMAGE-HD, PREDICT-HD and TRACK-HD, respectively.

Regions of interest

The regions of interest (ROI) considered for further analysis were the putamen, caudate, globus pallidus, nucleus accumbens, substantia nigra and thalamus, as well as the following cortical areas and white matter (WM) beneath them: precentral gyrus (PrCG, PrCWM), superior frontal gyrus (SFG, SFWM), superior parietal gyrus (SPG, SPWM), superior occipital gyrus (SOG, SOWM) and superior temporal gyrus (STG, STWM). The ROIs were selected for their consistent segmentation, as we attempted to analyse all regions. However, some regions of great interest such as the subthalamic nucleus and ventral diencephalon were not considered, as we found that their low contrast in T1-WIs of this dataset leads to less reliable segmentation. Brainstem was also not considered because the variable level of scan coverage could

introduce artifactual variations. ROIs in both hemispheres were considered together as there is little evidence for significant asymmetry in HD.

CAP score calculation

We aim to track the volume changes of each ROI over CAP scores among all three datasets (PREDICT-HD, TRACK-HD and IMAGE-HD). CAP scores were calculated across all three datasets by the following equation: $CAP = Age \times (CAG - 33.66)$, where Age represents the age of subjects in years and CAG represents the (constant) length of the individual's CAG repeat. A recent study²⁵ has shown that MRI scans of far-from-onset HD subjects are, with one exception, essentially indistinguishable from controls, so we included controls under 40 years old to model very far from onset HD in this study. The exception is that there are small differences in striatal volumes, which were attributed to early degeneration or to subtle developmental differences. Modification of the CAP equation for controls is described in the [supplementary material](#). Analyses were conducted with this modification or with the CAP score set at $CAP = Age$.

The regression model

In this study, we utilized a left-flat sigmoidal function and its statistical regression model, which are defined in detail in the [supplementary material](#), to capture the volume changes of each ROI over CAP scores. The rationale for this model is that most brain structure volumes in expansion-positive individuals far from onset are close to controls.²⁵ Therefore, for CAG expansion-positive individuals very far from predicted onset, and for controls under 40, volumes can be modelled,

as a first approximation, as constant. For all figures including controls, only controls under age 40 were used.

To reduce batch bias between datasets and subject groups, we considered datasets (PREDICT-HD, TRACK-HD and IMAGE-HD) and subject groups (i.e. controls, Pre-HD in Image-HD) as covariates in the statistical regression model. Subjects' groups are defined according to the clinical criteria specified in their original dataset. We also included Intracranial Volume (ICV) as a covariate.

For a second set of analyses, the volume of each ROI was also normalized to the whole brain volume before statistical regression model fitting. The ICV corresponds to the volume inside skull, including CSF and brain parenchyma, while the whole brain volume includes only the volume of brain tissue, without CSF. Therefore, whereas ICV reflects the head size, whole brain volume is representative of the overall parenchymal atrophy. For changepoint analysis, we used a semi-parametric bootstrap method to calculate the *P*-values.

Results

Table 1 shows the clinical characteristics of the subjects. For this plot, and all the others in the main figures, CAP score for controls is calculated as described in the supplemental text. (Additional details of the subjects and QC of the scans are shown in **Tables 1 and 2A and B** in the [supplementary material](#)).

Figure 1 shows the individual longitudinal clinical data ('spaghetti plots') of Total Motor Score (TMS), Symbol Digit Modalities Test (SDMT), Total Functional Capacity (TFC) and Beck Depression Inventory (BDI), where each of these were available, versus CAP score. As expected, inflection points in TMS and SDMT precede changes in TFC. Also, as expected, BDI (a reflection of depressive emotional

Table 1 Demographic, genetic and clinical characteristics of all participants at enrollment

Variable	Controls (n = 178) ^a			HD (n = 357) ^b			X ² (df)	P
	Mean	SD	Range	Mean	SD	Range		
Age (years)	45.2	11.0	22.6–71.9	43.6	11.3	18.6–71.6	2.0 (1)	0.161
CAP score ^c	252.9	61.6	126.6 to 402.7	377.9	89.6	149.6–631.6	200.4 (1)	<0.0001
CAG repeats	20.4	3.5	15 to 31	42.7	2.4	38–55	160.1 (1)	<0.0001
UHDRS-TMS	2.6	3.2	0 to 19	9.3	11.1	0–47	60.3 (1)	<0.0001
UHDRS-TFC	13.0	0.1	12 to 13	12.4	1.4	7–13	38.3 (1)	<0.0001
SDMT	53.8	9.6	28 to 80	46.9	13.3	12–80	35.1 (1)	<0.0001
BDI	4.8	5.3	0 to 22	6.4	7.2	0–43	1.7 (1)	0.195
Sex, male (%)		66 (37.1%)			149 (41.7%)		0.9 (1)	0.346
Study							0.3 (2)	0.881
IMAGE-HD		21 (11.8%)			42 (11.8%)			
PREDICT-HD		62 (34.8%)			132 (37.0%)			
TRACK-HD		95 (53.4%)			183 (51.3%)			

Comparison of HD and control participants in aggregate for the IMAGE-HD, PREDICT-HD and TRACK-HD studies. Only data from those participants whose imaging data (3 T only) passed the quality-control check are included. SD, standard deviation; X², Chi-square; df, degrees of freedom; CAP, CAG-Age Product; UHDRS, unified Huntington's disease rating scale; TMS, total motor score; TFC, total functional capacity; SDMT, symbol-digit modalities test and BDI, Beck depression inventory. X² values and corresponding *P*-values are from the Kruskal–Wallis test for continuous variables and the X² test for the nominal variable (sex).

^aFor control participants, CAG repeats were reported by PREDICT-HD only (n = 62), UHDRS by PREDICT-HD and TRACK-HD only (n = 157 for TMS and TFC), and BDI by PREDICT-HD and IMAGE-HD (n = 56).

^bFor HD participants, BDI was reported only by PREDICT-HD and IMAGE-HD (n = 122); UHDRS-TFC was reported only by PREDICT-HD and TRACK-HD (n = 312).

^cArbitrary value for CAP score for controls calculated as described in the text.

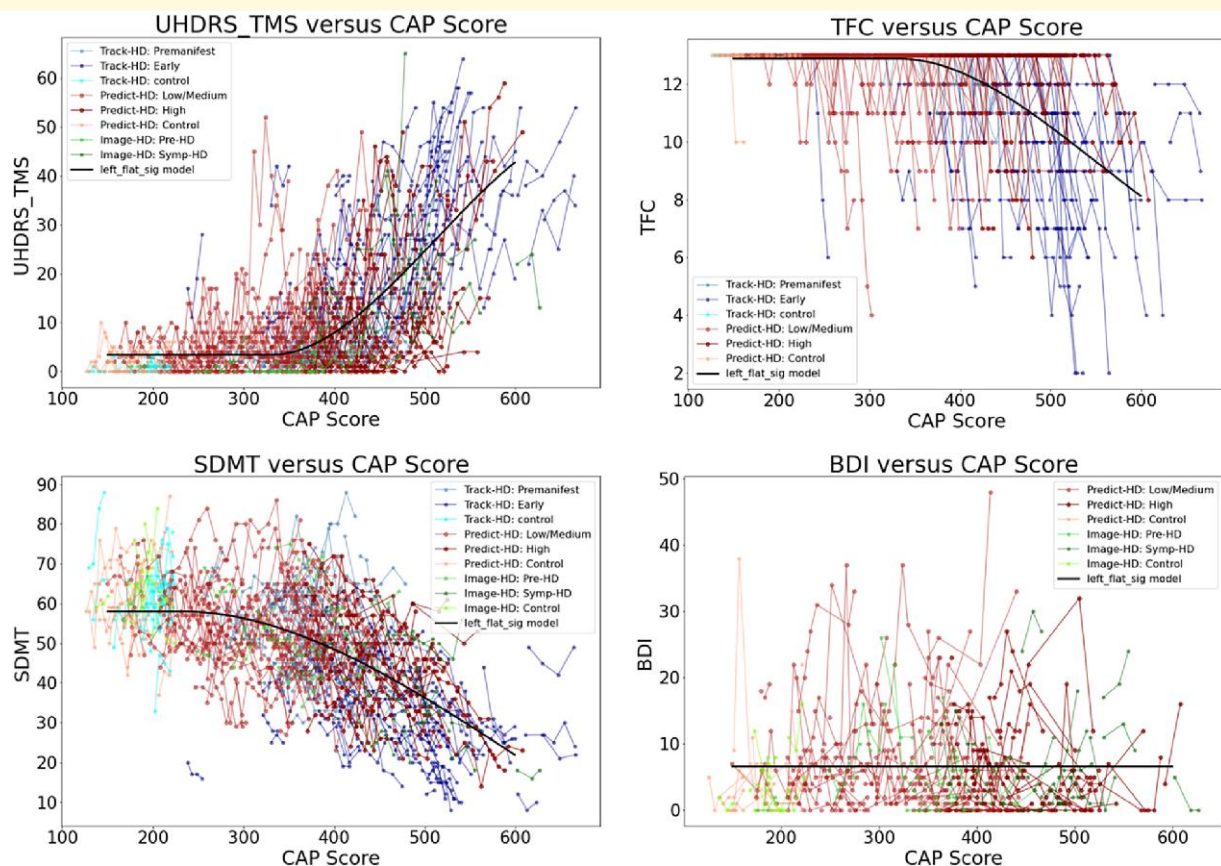


Figure 1 Individual longitudinal clinical data ('spaghetti plots') from all three studies (PREDICT, TRACK and IMAGE). TMS: total motor score; SDMT: symbol digit modalities test; TFC: total functional capacity; BDI: Beck depression inventory. Datasets appear in the following order: Track-HD: Premanifest, Track-HD: Early, Track-HD: control, Predict-HD: Low/Medium, Predict-HD: High, Predict-HD: Control, Image-HD: Pre-HD, Image-HD: Symp-HD, Left_flat_sig model. No available data for TFC from Image-HD and BDI from Track-HD.

state) shows no clear relationship to CAP score—emotional changes in HD do not occur with the predictability of motor or cognitive changes.

Figures 2 and 3 show the individual longitudinal volumetric data for selected regions ('spaghetti plots') from all three studies, plotted against CAP score. Intracranial volume is one of the covariates (but whole brain volume is not). Regions in the basal ganglia circuit have the most striking declines in volumes with greater CAP scores.

Figures 4 and 5 show individual longitudinal volumetric data for selected regions ('spaghetti plots') from all three studies, plotted against CAP score. Intracranial volume (ICV) is a covariate, as above, but here there is also normalization by whole brain volume. This analysis highlights the extent to which regions in the basal ganglia circuit have the most striking declines in volumes with greater CAP scores.

Figure 6 shows the summary trend lines for selected regions. A. Covariate intracranial volume only. B. Covariate intracranial volume plus normalization by whole brain volume. These comparisons highlight the extent to which regions in the basal ganglia circuit have the most striking declines in volumes with greater CAP scores, especially when normalized by whole brain volumes. Note that regions

whose relative volumes increase in Panel B do not have actual increase in volume—they just have less atrophy than the whole brain, i.e. they are relatively spared.

Supplemental Fig. 1 shows additional brain regions. Supplemental Fig. 2 shows additional brain regions, normalized by whole brain volume. Supplemental Fig. 3 shows analyses with control CAP = Age. Supplemental Fig. 4 provides the CAP score at first slope change for the sigmoidal model applied to each volume, and its standard deviation. Only volumes for which the sigmoid fitting was better than a linear model are listed. A provides results for covariate intracranial volume only and B for normalized by whole brain volume. Results in both cases indicate an earlier changepoint for putamen and caudate, followed by a group of structures that include the globus pallidus, the nucleus accumbens and the white matter in the precentral cortex. Several of the changes detected in un-normalized volumes lose their significance after normalization, suggesting that these changes are in part due to global brain volume loss.

Since analyses by CAP scores including controls require somewhat arbitrary methods to assign controls a CAP score, we also conducted analyses using HD cases only. Figures 7–10 show similar analyses with CAG expansion cases only, no controls. Supplemental Figs 5 and 6 show

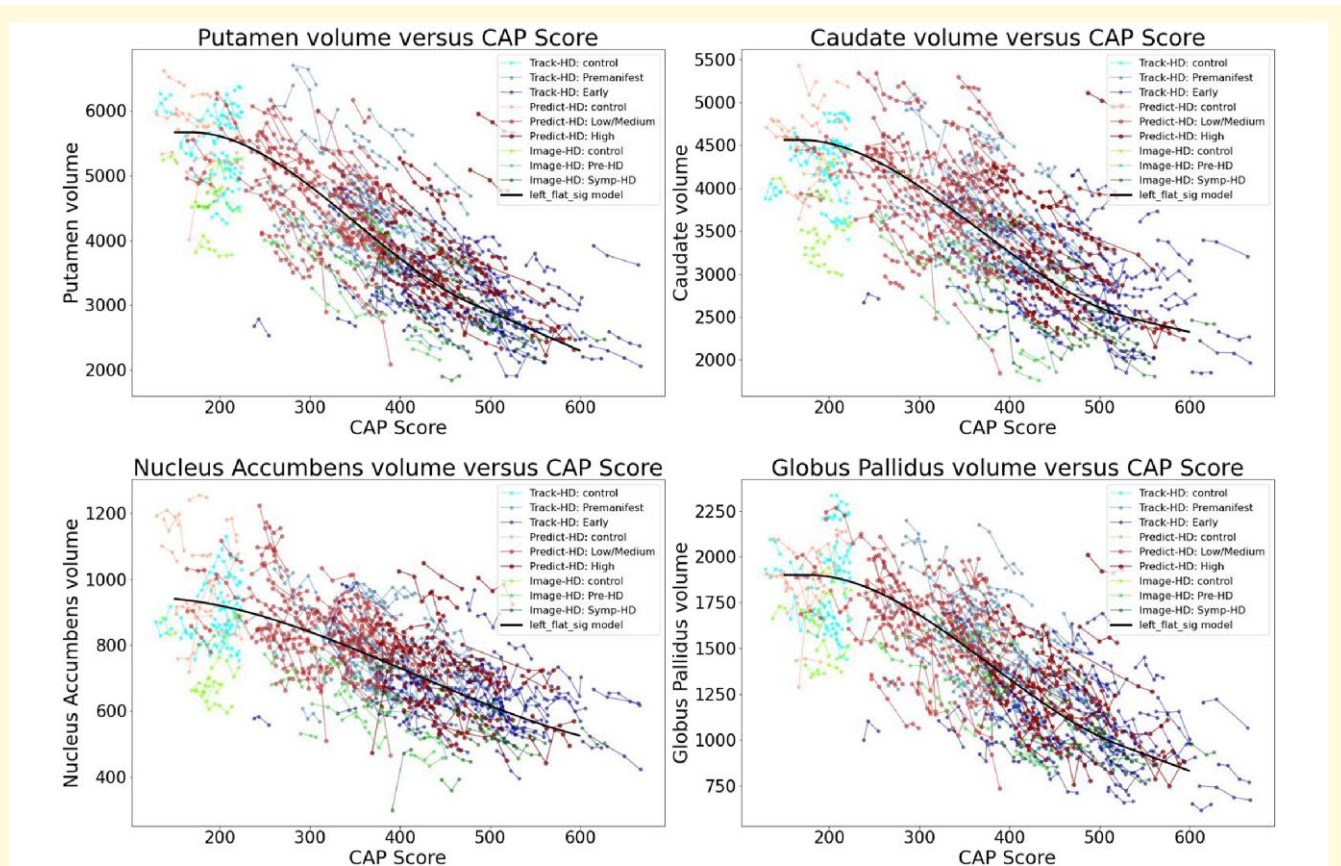


Figure 2 Individual longitudinal volumetric data for selected regions ('spaghetti plots') from all three studies (PREDICT, TRACK and IMAGE), plotted by CAP score. Covariate intracranial volume only (CAG expansion positive individuals and controls < age 40). Regions in the basal ganglia circuit have the most striking declines in volumes with greater CAP scores. Datasets appear in the following order: Track-HD: control, Track-HD: Premanifest, Track-HD: Early, Predict-HD: control, Predict-HD: Low/Medium, Predict-HD: High, Image-HD: control, Image-HD: Pre-HD, Image-HD: Symp-HD, Left_flat_sig model.

analyses of additional brain regions. Figure 11 shows trend lines for CAG expansion subjects only. These analyses also indicate preferential atrophy of the structures in the basal ganglia circuit.

Discussion

These data highlight the selective vulnerability to progressive atrophy in HD of subcortical regions in the basal ganglia circuit. They raise the interesting possibility that there are circuit-based processes underlying regional brain atrophy in HD. As expected, the striatum has profound selective, early degeneration. Other regions of the brain within the striatal circuit also have selective severe degeneration. The globus pallidus in particular has severity of degeneration comparable to that of the striatum. In addition, regions in the basal ganglia circuit such as the nucleus accumbens and substantia nigra also have preferential atrophy. By contrast, most of the other brain regions examined appear to undergo slow but steady atrophy within a narrower range, with some being relatively spared.

A great strength of the study is the analysis of the large number of structural MRI images using the same analytic pipeline.¹⁵ This permits the combining of different datasets, and enhances the generalizability of the results. To our knowledge, this study represents the most comprehensive delineation of the natural history of regional brain atrophy in HD to date, combining TRACK, PREDICT and IMAGE participants. We encapsulated an extensive list of brain regions and showed individual trend lines to underscore selective alteration of the basal ganglia circuitry during disease progression. We also identified the time course of slope change for regions of interest, which highlights early striatal degeneration.

Another great strength is that the combination of the three datasets includes subjects with a wide range of CAP scores. Most subjects were relatively early in the course of HD, i.e. in the premanifest period, though some started in the manifest period, and some 'converted' to motor manifest HD²⁶ during the course of the study. Diagnosis of HD in these studies was made using clinician assessment of motor signs using the unified Huntington's disease rating scale (UHDRS),³ not the more recent incorporation of cognitive changes.⁴ Thus,

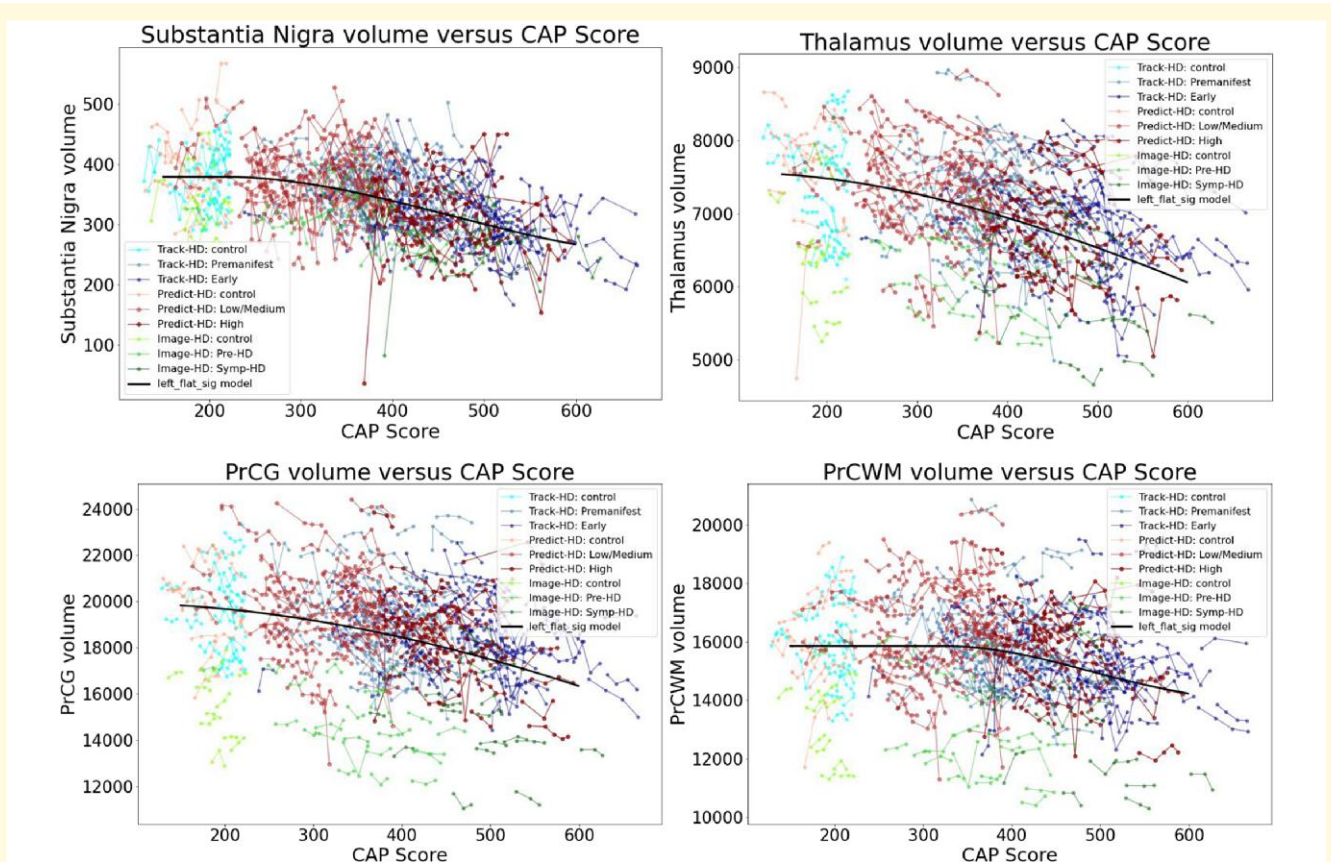


Figure 3 Individual longitudinal volumetric data for selected regions (‘spaghetti plots’) from all three studies (PREDICT, TRACK and IMAGE), plotted by CAP score. Covariate intracranial volume only (CAG expansion positive individuals and controls < age 40). Regions in the basal ganglia circuit have the most striking declines in volumes with greater CAP scores. Refer to Fig. 2 for complete dataset list.

overall there is a range of subject CAP scores, covering well the key period of early to moderate brain atrophy, which would not have been available studying any single dataset.

However, there are a number of limitations which must be acknowledged. The automated analysis platform,¹⁵ while highly sophisticated and capable of dealing with selective regional brain atrophy due to the use of the LDDMM method, does not have the face validity of expert manual segmentation for each individual region. However, it would be impossible to analyse so many scans without automated image analysis. As described in the methods, all scans did have manual quality control. Another segmentation issue, faced by both humans and computational methods, is that small regions, and those with relatively low contrast, may be especially liable to inconsistent results. Therefore, the results must be interpreted in the light of the regional segmentation reliability.²⁴ There are some important regions which were too small or too uncertain to segment and were not included, such as the brain stem, subthalamic nucleus and ventral diencephalon. There is little evidence of asymmetric atrophy in HD, so our study did not analyse the two hemispheres separately, though this could be explored in the future if felt to be desirable. Furthermore, our results are limited to volumetric analysis. Other methods such as voxel-based morphometry, or other

morphometry-based techniques might give complementary results.^{27–29}

Other limitations involve the range of CAP scores. Our trend lines are limited to the range of CAP scores between 200 and 600, because we do not have sufficient data outside of that range. These studies did not include images from HD individuals with severe disease, who are often difficult to scan because of involuntary movements or other clinical issues. In addition, there is a lack of individuals very far from predicted onset.

Because of the recent important study from Scahill *et al.*,²⁵ we know that individuals very far from onset have most regional volumes essentially equivalent to normal, with the exception of slight but significant differences in striatal volumes; therefore, we have used the expedient introduction of normal controls into the analysis in order to overcome this limitation. The slightly different striatal volumes in the very far-from-onset individuals²⁵ could be due to atrophy beginning even earlier in the natural history of HD or due to a contribution from developmental differences in HD^{30–33} or possibly both. If the former is correct, then the use of controls as surrogates for very far-from-onset subjects will give a good overall description of the extent of atrophy. If the latter is correct, then our striatal data should be interpreted as

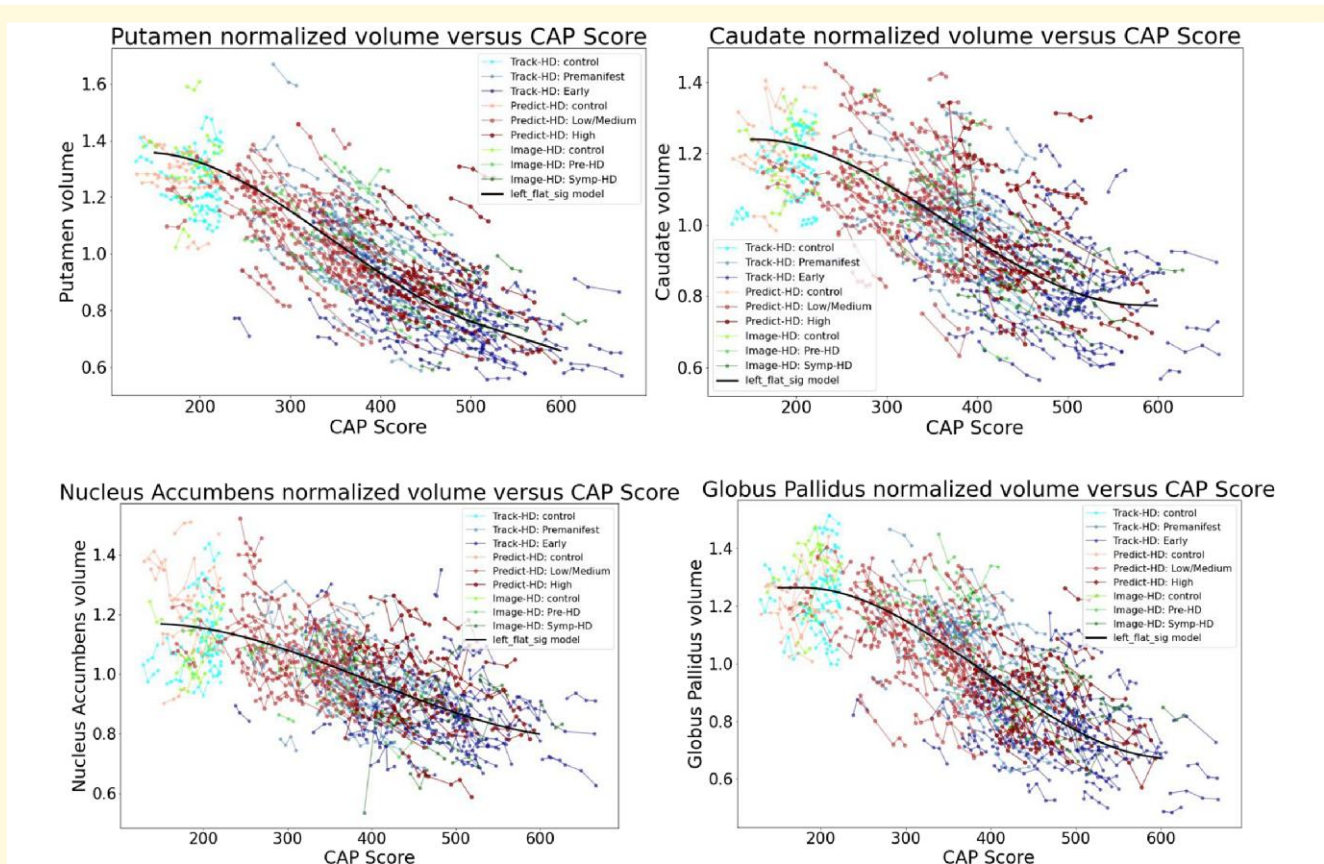


Figure 4 Individual longitudinal volumetric data for selected regions ('spaghetti plots') from all three studies (PREDICT, TRACK and IMAGE), plotted by CAP score. Covariate intracranial volume, plus normalization by whole brain volume (CAG expansion positive individuals and controls < age 40). This analysis highlights the extent to which regions in the basal ganglia circuit have the most striking declines in volumes with greater CAP scores. Refer to Fig. 2 for complete dataset list.

reflecting a combination of a small component of developmental differences, plus the major component of degeneration. Because of the lack of a large number of subjects with CAP less than 200, it is difficult to define the CAP scores at which atrophy begins, so we do not attempt to draw conclusions here about the initiation of atrophy in different regions.

The use of the multiplier to assign the control subjects the equivalent of a CAP score is arbitrary. However, it helps to spread their data out over a larger range of scores. The goal of the study was to compare the relationship of atrophy of different brain regions in the HD subjects with CAP scores, and the use of the controls to substitute for very far from onset subjects will apply to all brain regions equally. We show that the overall patterns of results are very comparable using control CAP = Age (supplemental Fig. 3) or analysing the CAG expansion subjects only (Figs 5–7) without inclusion of controls.

Our results are broadly similar to those of Wijeratne *et al.*,¹⁶ though we have emphasized longitudinal trajectory (including with normalization for total brain volume), rather than effect sizes and markers and power for clinical trials. Technical differences include the analytic pipelines used,

and the inclusion of the 1.5 T scans from PREDICT in their study, but not in the current study. Another study of Wijeratne *et al.*³⁴ detected early changes in subcortical regions of the striatum using the Gaussian process progression model but with only TRACK and PREDICT participants, whereas we included the IMAGE study and a more thorough list of brain regions to demonstrate evidence of circuitry-based atrophy. They confirmed that structural brain atrophy provides improved prediction of onset of manifest HD, as previously shown in the PREDICT dataset alone.²⁶ While they state that 'monotonicity in the group-level volumetric evolution was enforced,' nevertheless, their model, which involves many degrees of freedom, has the curves changing direction (for instance, caudate turns up towards the end, while lateral ventricle turns down), which does not fit the biology of HD. We believe that the sigmoid function that we used provides a better reflection of the progressive monotonic but non-linear nature of neurodegeneration in HD, and we show that it provides a statistically superior fit to the data compared to a linear model. Our results are also congruent with those of Abeyasinghe *et al.*,³⁵ though their focus on describing trajectories (using Freesurfer) for subjects with different CAP scores was very different from the current one.

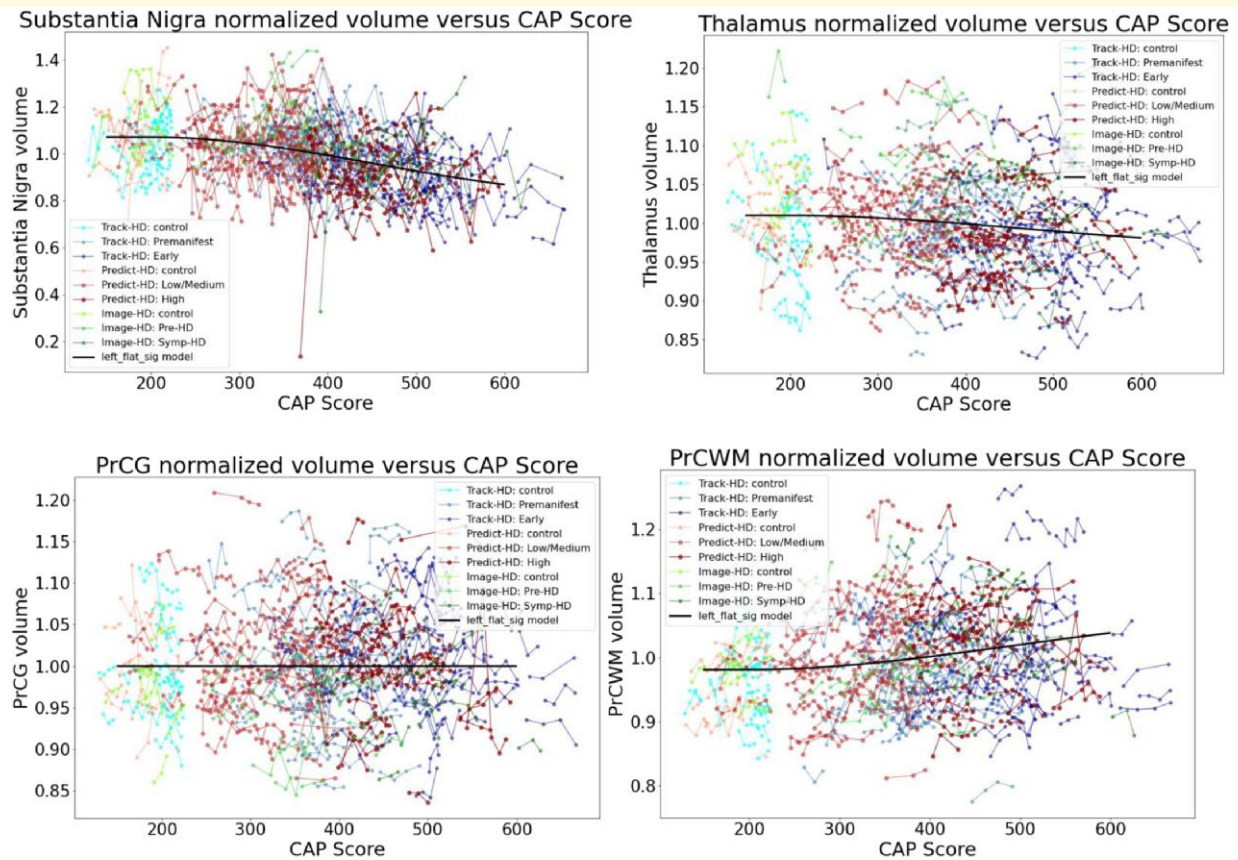


Figure 5 Individual longitudinal volumetric data for selected regions ('spaghetti plots') from all three studies (PREDICT, TRACK and IMAGE), plotted by CAP score. Covariate intracranial volume, plus normalization by whole brain volume (CAG expansion positive individuals and controls < age 40). This analysis highlights the extent to which regions in the basal ganglia circuit have the most striking declines in volumes with greater CAP scores. Refer to Fig. 2 for complete dataset list.

They found that striatal volumes alone captured much of the variance in disease progression expressed by clinical variables, highlighting the importance of imaging as a potential outcome measure for clinical trials. It would be interesting to compare the results of the analyses in this study with similar analyses of Freesurfer data or other analytic pipelines.

Most regions of the brain, including many regions shown in the [supplementary data](#), appear to undergo slow but steady atrophy over the longitudinal course of HD. By contrast, the striatum and other regions in the basal ganglia circuit undergo preferentially severe degeneration. This suggests the possibility of two mechanisms underlying neuronal degeneration in HD—perhaps all regions of the brain are affected by cell-autonomous mechanisms with roughly equivalent rates of atrophy, including white matter regions.³⁶ This would be consistent with many animal model studies showing that not just neurons but other cells can contribute to HD pathogenesis. The cerebellum is sometimes thought of as a control region relatively unaffected by HD. However, our data suggest that cerebellum, while one of the relatively less affected regions, is within the broad group of regions undergoing slow but steady atrophy, and for instance is quite comparable to the hippocampus.

While these regions have relatively steady atrophy, there is substantial variation from case to case, so there are likely to be many opportunities for more detailed study of individual regions, and for clinical correlations, as have been done in the individual datasets. For instance, regional cortical atrophy has been shown in each dataset individually.^{12,37,38} For the cortex, thickness may be more revealing than volumetric analysis, but even in the current study using cortical volumes, there appear to be differences in different regions. Newer methods of analysing cortical thickness³⁹ may be useful for clinical correlations. Also, subcortical regions may have interesting correlations. For instance, amygdala atrophy was correlated with depression in the IMAGE dataset.⁴⁰ This finding suggests different HD phenotypes may be associated with alterations of specific structures, apparent at various timepoints throughout disease progression, not all of which are revealed in our study.

By contrast the striatum and other regions within the basal ganglia circuit undergo preferential and more profound degeneration. The basal ganglia selectivity raises the possibility of pathogenesis dependent on neuronal circuits, as has been suggested previously.^{1,41–44} Excitotoxicity has long been believed to contribute to HD pathogenesis in the striatum.⁴⁵

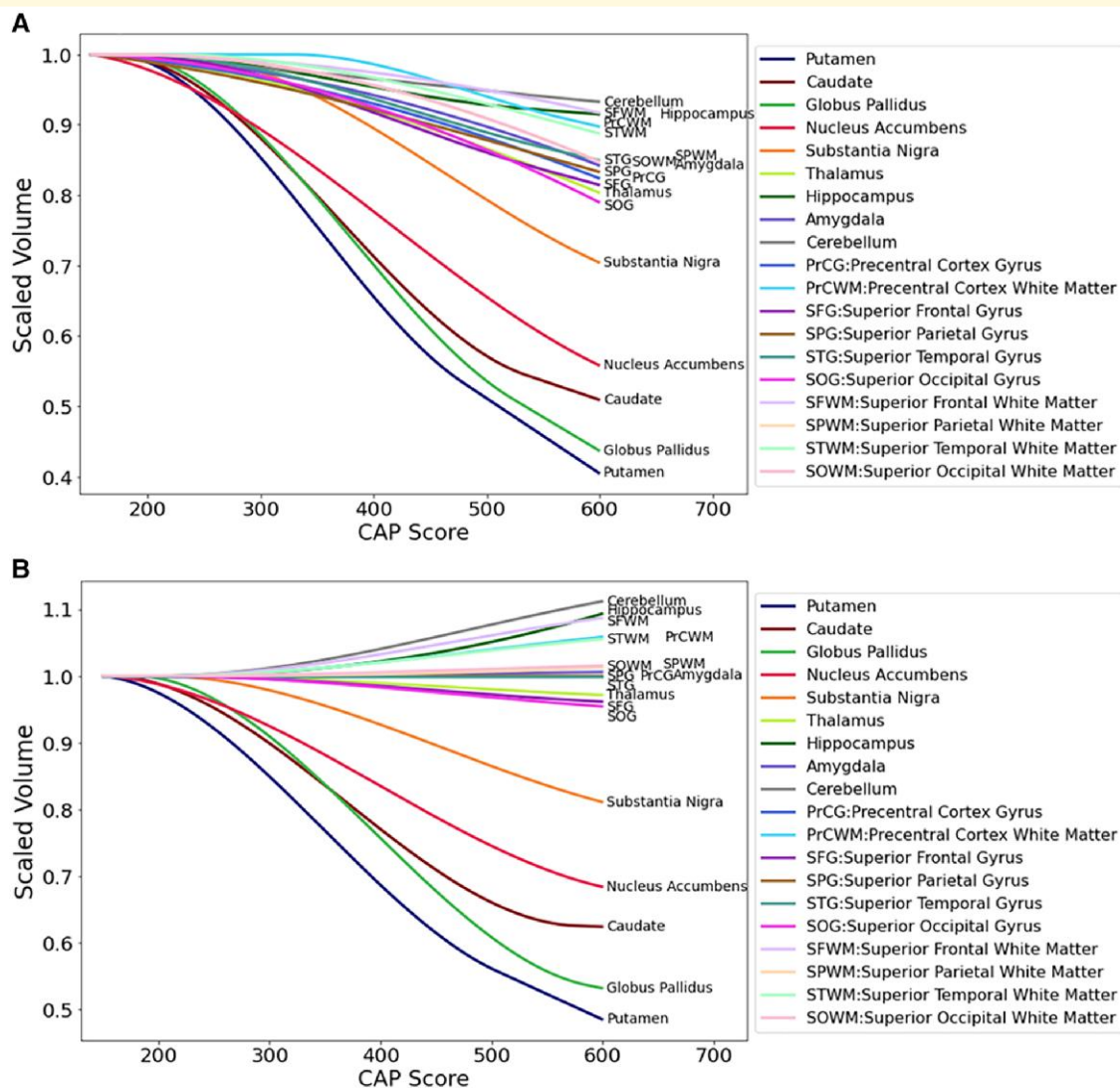


Figure 6 Summary trend lines for selected regions. (A) Covariate intracranial volume only (CAG expansion positive and controls < age 40). **(B)** Covariate intracranial volume and normalized by whole brain volume (CAG expansion positive and controls < age 40). These comparisons highlight the extent to which regions in the basal ganglia circuit have the most striking declines in volumes with greater CAP scores, especially when normalized by whole brain volumes. Note that regions whose relative volumes increase in Panel **(B)** do not have actual increase in volume—they just have less atrophy than the whole brain, i.e. they are relatively spared.

There is considerable evidence for excitotoxic injury in HD.⁴⁶ The severe involvement of the globus pallidus would appear inconsistent with excitotoxicity. The projection from the cortex to the striatum provides massive glutamatergic input to medium spiny neurons, and thus could be a substrate for excitotoxicity. However, the projection from the striatum to the globus pallidus is purely comprised of inhibitory neurons using GABA as a transmitter. Thus, excitotoxicity would not be possible for this synaptic interaction, though it is conceivable that glutamatergic innervation from the subthalamic nucleus⁴⁷ could contribute. It must be acknowledged that the pallidum has relatively few neurons compared to the striatum,⁴⁸ so it may be that atrophy there results from massive loss of afferent terminals as well as neuronal loss.⁴⁹ White matter pathology has been well

established in HD.^{50–54} The thalamus receives basal ganglia projections, but is not preferentially affected; however, it has many nuclei that do not receive basal ganglia projections, so a subnuclear or shape analysis may be more revealing.

Another mechanism might involve prion-like transmission of mutant Htt from one neuron to another. Network-based preferential atrophy and the mechanism of prion-like transmission have been proposed in Parkinson's disease and Alzheimer's disease,^{28,55,56} as well as of course in prion disease,^{57,58} though it may not be the only explanation for circuit-based atrophy. There are some striking data that favour this mechanism for HD as well, including in-vitro and in-vivo experiments, and observation of human postmortem brain material from transplant studies.^{59–65} Other potential mechanisms include loss of growth factor transport, or

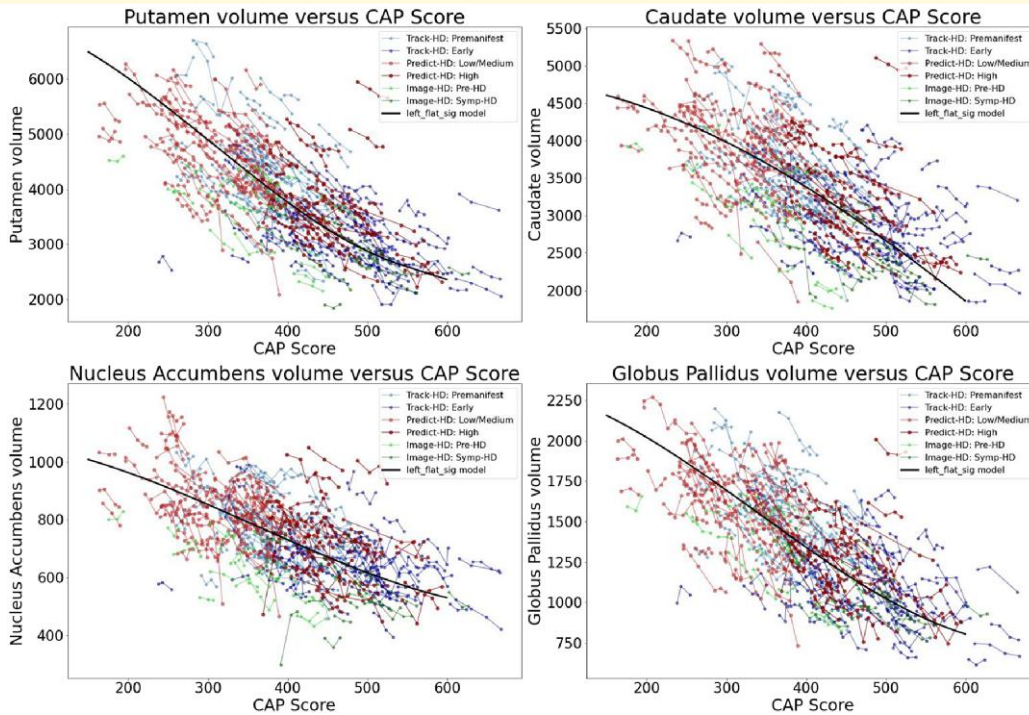


Figure 7 Individual longitudinal volumetric data ('spaghetti plot') for selected regions. Covariate intracranial volume only (CAG expansion positive only, no controls). Datasets appear in the following order: Track-HD: Premanifest, Track-HD: Early, Predict-HD: Low/Medium, Predict-HD: High, Image-HD: Pre-HD, Image-HD: Symp-HD, Left_flat_sig model.

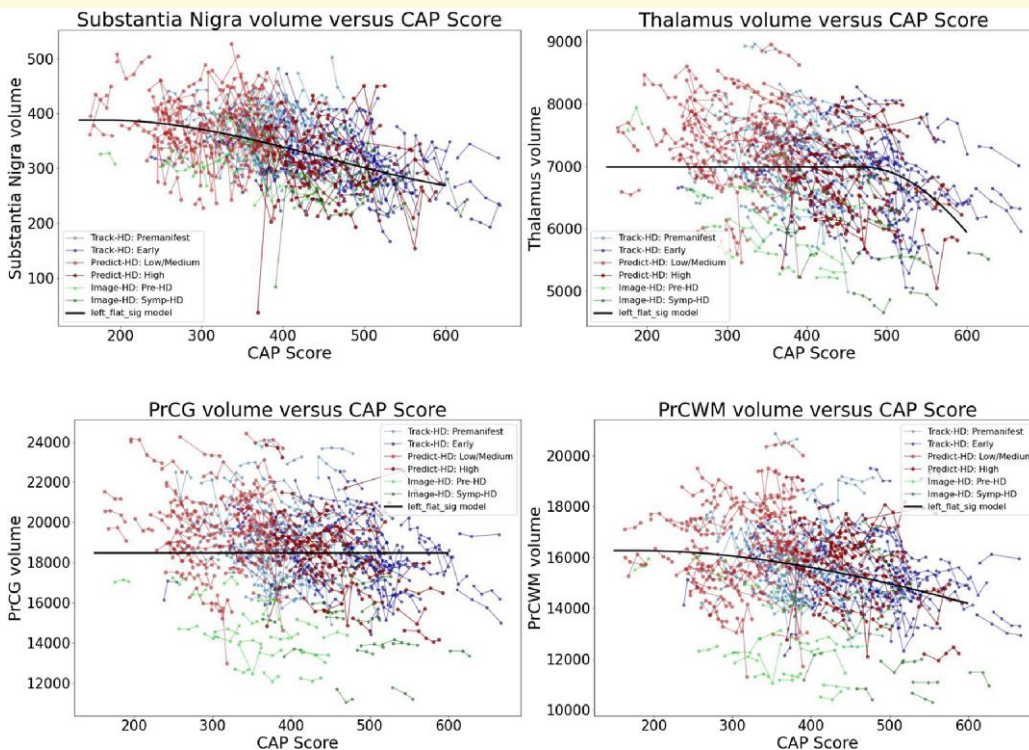


Figure 8 Individual longitudinal volumetric data ('spaghetti plot') for selected regions. Covariate intracranial volume only (CAG expansion positive only, no controls). Refer to Fig. 7 for complete dataset list.

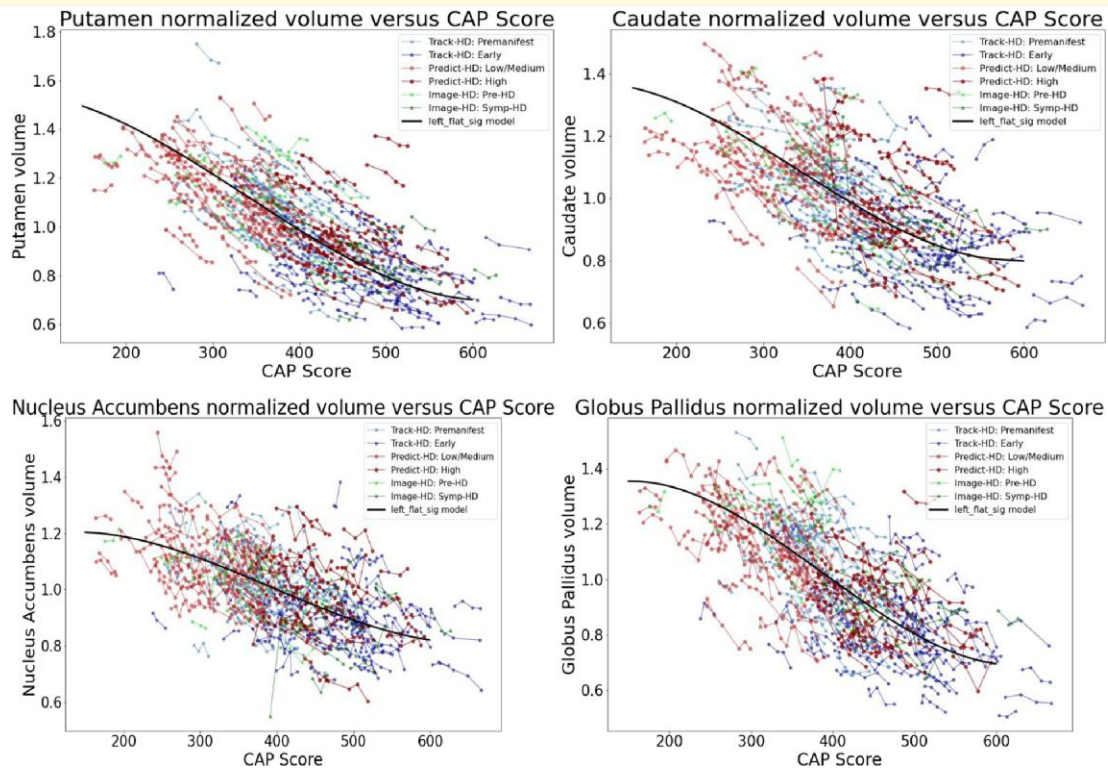


Figure 9 Individual longitudinal volumetric data ('spaghetti plot') for selected regions. Covariate intracranial volume, plus normalization by whole brain volume (CAG expansion positive only, no controls). Refer to Fig. 7 for complete dataset list.

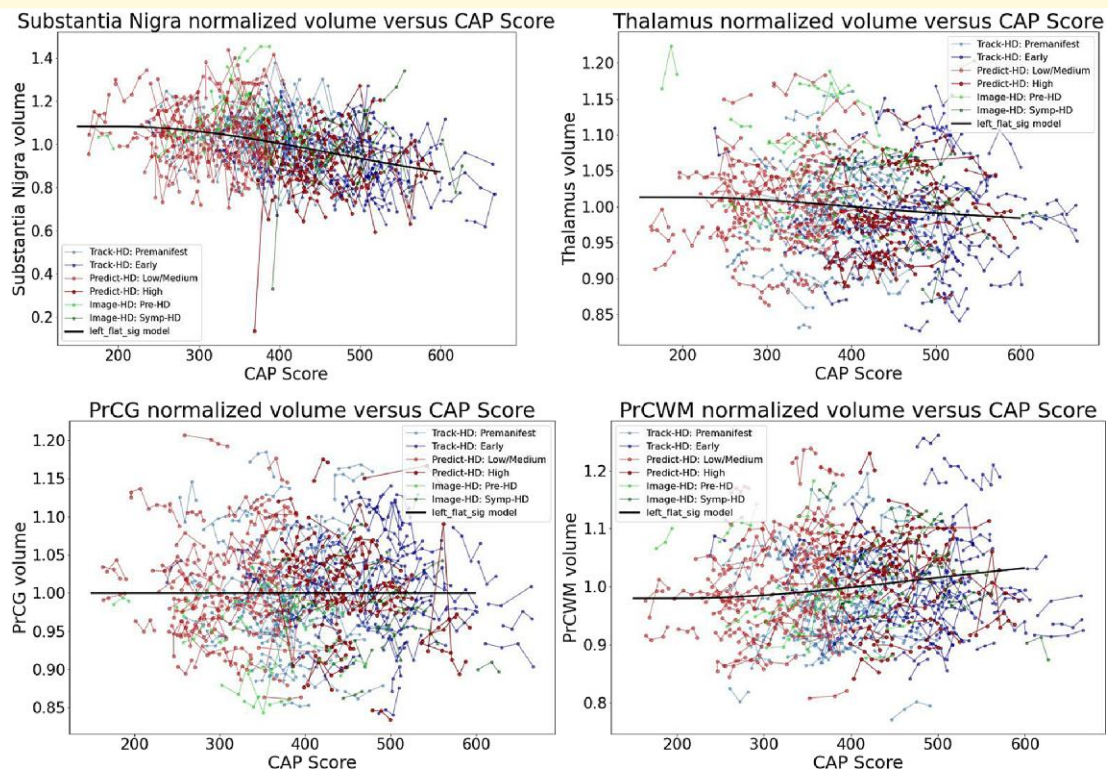


Figure 10 Individual longitudinal volumetric data ('spaghetti plot') for selected regions. Covariate intracranial volume, plus normalization by whole brain volume (CAG expansion positive only, no controls). Refer to Fig. 7 for complete dataset list.

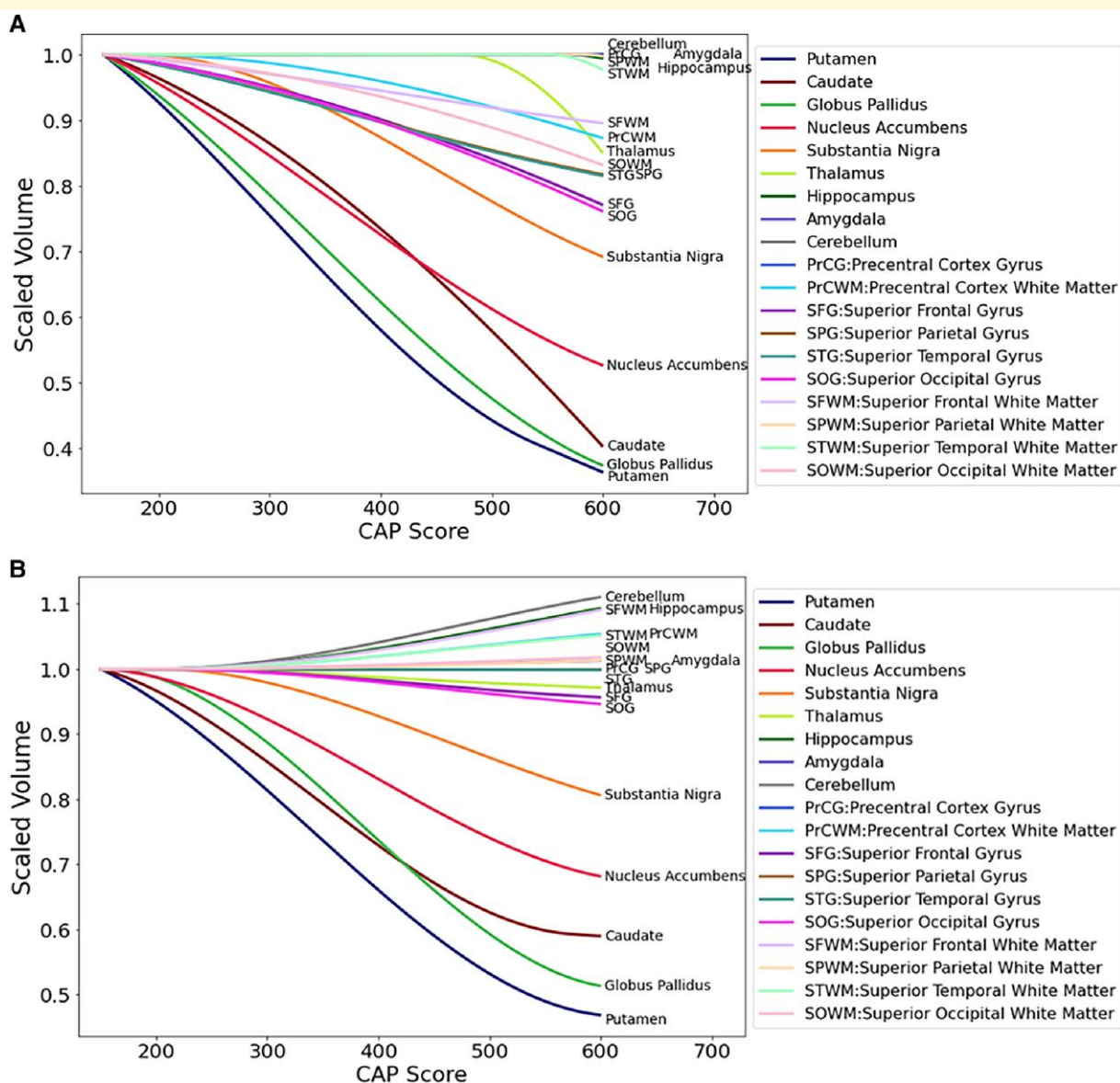


Figure 11 Summary trend lines for selected regions, CAG expansion positive only, no controls. (A) Covariate intracranial volume only. (B) Covariate intracranial volume, plus normalization by whole brain volume. These analyses also indicate preferential atrophy of the structures in the basal ganglia circuit.

altered synaptic connectivity,^{1,66–68} perhaps due to abnormal complement-mediated pruning.⁶⁹ The recent identification of modifier genes involved in DNA repair has led to hypotheses based on somatic expansion of the CAG repeat.^{70,71} The regional variation in somatic expansions⁷² appears to match the regional variation in extent of atrophy; though more detailed studies of this relationship could be revealing. Thus, the apparent circuit-based preferential pathology could have several explanations, as has also been proposed for PD.⁷³ Furthermore, other mechanisms, such as cell-autonomous effects, must explain the overall atrophy present in later stage cases of HD, especially in juvenile onset HD.⁷⁴

In conclusion, these data provide a comprehensive description of the natural history of regional volumetric brain

atrophy in HD. They highlight the widespread degeneration of many (and perhaps all) regions of brain over the course of HD. They also highlight the selective atrophy of regions in the basal ganglia circuit, with implications for pathogenesis and experimental therapeutics. These results support (though certainly do not prove) the hypothesis of circuit-based spread of pathology in HD, possibly due to spread of mutant Htt protein, supporting therapeutic targets related to prion-like spread of pathology or other connection-based mechanisms. In addition, they have implications for current neurosurgical therapeutic approaches, since delivery of therapeutic agents solely to the caudate and putamen may miss structures affected early, such as nucleus accumbens, and output nuclei of the striatum, the substantia nigra and globus pallidus.

Supplementary material

Supplementary material is available at *Brain Communications* online.

Acknowledgements

We thank CHDI for maintaining and transmitting (Darren Freeman) the datasets for these analyses. We thank the anonymous peer reviewers for helpful suggestions and references, which we have incorporated into the discussion. We would like to acknowledge the contribution of all the participants who took part in this study. We are also grateful to the CHDI Foundation Inc. (grant number A—3433), New York (USA), and to the National Health and Medical Research Council (NHMRC) (grant number 606650) for their support in funding this research. We also thank the Royal Children's Hospital for the use of their 3 T MR scanner.

Funding

This work was supported by National Institute of Neurological Disorders and Stroke (NS102670-01A1 and NS086452-06) (plus grants supporting the generation of the original datasets, as noted in their publications cited). Dr. Ross is also supported by R01NS086452. Dr. Miller, Faria, and Ratnanather are supported by National Institutes of Health (P41-EB031771).

Conflict of interests

Funding for the study was provided by the NIH under a license agreement between AnatomyWorks LLC and the Johns Hopkins University. Dr. Michael I. Miller and the University are entitled to royalty distributions related to technology described in the study. Dr. Miller is a founder of and holds equity in AnatomyWorks LLC. This arrangement has been reviewed and approved by the Johns Hopkins University in accordance with its conflict of interest policies. The other authors declare no relevant conflicts of interest.

Data availability

The study is ongoing with the images still under analysis. The individual brain regional volumetric data reported here will be provided to qualified investigators upon request and discussion.

References

- Ross CA, Aylward EH, Wild EJ, *et al.* Huntington disease: Natural history, biomarkers and prospects for therapeutics. *Nat Rev Neurol.* 2014;10(4):204-216.
- Tabrizi SJ, Flower MD, Ross CA, Wild EJ. Huntington disease: New insights into molecular pathogenesis and therapeutic opportunities. *Nat Rev Neurol.* 2020;16(10):529-546.
- Unified Huntington's disease rating scale: Reliability and consistency. Huntington study group. *Mov Disord* 1996;11(2):136-142.
- Ross CA, Reilmann R, Cardoso F, *et al.* Movement disorder society task force viewpoint: Huntington's disease diagnostic categories. *Mov Disord Clin Pract.* 2019;6(7):541-546.
- Penney JB Jr, Vonsattel JP, MacDonald ME, Gusella JF, Myers RH. CAG Repeat number governs the development rate of pathology in Huntington's disease. *Ann Neurol.* 1997;41(5):689-692.
- Zhang Y, Long JD, Mills JA, *et al.* Indexing disease progression at study entry with individuals at-risk for Huntington disease. *Am J Med Genet B Neuropsychiatr Genet.* 2011;156B(7):751-763.
- Vonsattel JP, Myers RH, Stevens TJ, Ferrante RJ, Bird ED, Richardson EP Jr. Neuropathological classification of Huntington's disease. *J Neuropathol Exp Neurol.* 1985;44(6):559-577.
- Rub U, Seidel K, Heinsen H, Vonsattel JP, den Dunnen WF, Korf HW. Huntington's disease (HD): The neuropathology of a multisystem neurodegenerative disorder of the human brain. *Brain Pathol.* 2016;26(6):726-740.
- Aylward EH, Sparks BF, Field KM, *et al.* Onset and rate of striatal atrophy in preclinical Huntington disease. *Neurology.* 2004;63(1):66-72.
- Paulsen JS, Long JD, Ross CA, *et al.* Prediction of manifest Huntington's disease with clinical and imaging measures: A prospective observational study. *Lancet Neurol.* 2014;13(12):1193-1201.
- Tabrizi SJ, Scahill RI, Owen G, *et al.* Predictors of phenotypic progression and disease onset in premanifest and early-stage Huntington's disease in the TRACK-HD study: Analysis of 36-month observational data. *Lancet Neurol.* 2013;12(7):637-649.
- Dominguez D JF, Stout JC, Poudel G, *et al.* Multimodal imaging biomarkers in premanifest and early Huntington's disease: 30-month IMAGE-HD data. *Br J Psychiatry.* 2016;208(6):571-578.
- Aylward EH, Harrington DL, Mills JA, *et al.* Regional atrophy associated with cognitive and motor function in prodromal Huntington disease. *J Huntingtons Dis.* 2013;2(4):477-489.
- Paulsen JS, Langbehn DR, Stout JC, *et al.* Detection of Huntington's disease decades before diagnosis: The predict-HD study. *J Neurol Neurosurg Psychiatry.* 2008;79(8):874-880.
- Mori SWD, Ceritoglu C, Li Y, *et al.* MRICloud: Delivering high-throughput MRI neuroinformatics as cloud-based software as a service. *Comput Sci Eng.* 2016;18(5):21-35.
- Wijeratne PA, Johnson EB, Eshaghi A, *et al.* Robust markers and sample sizes for multicenter trials of Huntington disease. *Ann Neurol.* 2020;87(5):751-762.
- Tang X, Oishi K, Faria AV, *et al.* Bayesian parameter estimation and segmentation in the multi-atlas random orbit model. *PLoS One.* 2013;8(6):e65591.
- Tang X, Crocetti D, Kutten K, *et al.* Segmentation of brain magnetic resonance images based on multi-atlas likelihood fusion: Testing using data with a broad range of anatomical and photometric profiles. *Front Neurosci.* 2015;9:61.
- Beg MFM, Trouvé A, Younes L. Computing large deformation metric mappings via geodesic flows of diffeomorphisms. *Int J Comput Vis.* 2005;61:139-157.
- Ma J, Ma HT, Li H, *et al.* A fast atlas pre-selection procedure for multi-atlas based brain segmentation. *Annu Int Conf IEEE Eng Med Biol Soc.* 2015;2015:3053-3056.
- Wu D, Ma T, Ceritoglu C, *et al.* Resource atlases for multi-atlas brain segmentations with multiple ontology levels based on T1-weighted MRI. *Neuroimage.* 2016;125:120-130.
- Liang Z, He X, Ceritoglu C, *et al.* Evaluation of cross-protocol stability of a fully automated brain multi-atlas parcellation tool. *PLoS One.* 2015;10(7):e0133533.
- Ceritoglu C, Tang X, Chow M, *et al.* Computational analysis of LDDMM for brain mapping. *Front Neurosci.* 2013;7:151.

24. Rezende TJR, Campos BM, Hsu J, *et al.* Test-retest reproducibility of a multi-atlas automated segmentation tool on multimodality brain MRI. *Brain Behav.* 2019;9(10):e01363.
25. Scahill RI, Zeun P, Osborne-Crowley K, *et al.* Biological and clinical characteristics of gene carriers far from predicted onset in the Huntington's disease young adult study (HD-YAS): A cross-sectional analysis. *Lancet Neurol.* 2020;19(6):502-512.
26. Aylward EH, Liu D, Nopoulos PC, *et al.* Striatal volume contributes to the prediction of onset of Huntington disease in incident cases. *Biol Psychiatry.* 2012;71(9):822-828.
27. Manera AL, Dadar M, Collins DL, Ducharme S; Frontotemporal lobar degeneration neuroimaging initiative. Deformation based morphometry study of longitudinal MRI changes in behavioral variant frontotemporal dementia. *Neuroimage Clin.* 2019;24:102079.
28. Pieperhoff P, Südmeyer M, Dinkelbach L, *et al.* Regional changes of brain structure during progression of idiopathic Parkinson's disease —A longitudinal study using deformation based morphometry. *Cortex.* 2022;151:188-210.
29. Zeighami Y, Fereshtehnejad SM, Dadar M, *et al.* A clinical-anatomical signature of Parkinson's disease identified with partial least squares and magnetic resonance imaging. *Neuroimage.* 2019;190:69-78.
30. Nopoulos PC, Aylward EH, Ross CA, *et al.* Smaller intracranial volume in prodromal Huntington's disease: Evidence for abnormal neurodevelopment. *Brain.* 2011;134(Pt 1):137-142.
31. van der Plas E, Langbehn DR, Conrad AL, *et al.* Abnormal brain development in child and adolescent carriers of mutant huntingtin. *Neurology.* 2019;93(10):e1021-e1030.
32. van der Plas E, Schultz JL, Nopoulos PC. The neurodevelopmental hypothesis of Huntington's disease. *J Huntingtons Dis.* 2020;9(3): 217-229.
33. Zhang C, Wu Q, Liu H, *et al.* Abnormal brain development in Huntington' disease is recapitulated in the zQ175 knock-in mouse model. *Cereb Cortex Commun.* 2020;1(1): tga044.
34. Wijeratne PA, Garbarino S, Gregory S, *et al.* Revealing the timeline of structural MRI changes in premanifest to manifest Huntington disease. *Neurol Genet.* 2021;7(5):e617.
35. Abeyasinghe PM, Long JD, Razi A, *et al.* Tracking Huntington's disease progression using motor, functional, cognitive, and imaging markers. *Mov Disord.* 2021;36(10):2282-2292.
36. Creus-Muncunill J, Ehrlich ME. Cell-autonomous and non-cell-autonomous pathogenic mechanisms in Huntington's disease: Insights from in vitro and in vivo models. *Neurotherapeutics.* 2019;16(4):957-978.
37. Nopoulos PC, Aylward EH, Ross CA, *et al.* Cerebral cortex structure in prodromal Huntington disease. *Neurobiol Dis.* 2010; 40(3):544-554.
38. Hobbs NZ, Pedrick AV, Say MJ, *et al.* The structural involvement of the cingulate cortex in premanifest and early Huntington's disease. *Mov Disord.* 2011;26(9):1684-1690.
39. Ratnanather JT, Kutten KS, Hubka P, Kral A, Younes L. 3D normal coordinate systems for cortical areas. In: Kushnarev S, Qiu A, Younes L, eds. *Mathematics of shapes and applications* (Lecture Notes Series). Institute of Mathematical Sciences, National University of Singapore; 2019.
40. Ahveninen LM, Stout JC, Georgiou-Karistianis N, Lorenzetti V, Glikmann-Johnston Y. Reduced amygdala volumes are related to motor and cognitive signs in Huntington's disease: The IMAGE-HD study. *Neuroimage Clin.* 2018;18:881-887.
41. Poudel GR, Stout JC, Dominguez DJ, *et al.* White matter connectivity reflects clinical and cognitive status in Huntington's disease. *Neurobiol Dis.* 2014;65:180-187.
42. Poudel GR, Harding IH, Egan GF, Georgiou-Karistianis N. Network spread determines severity of degeneration and disconnection in Huntington's disease. *Hum Brain Mapp.* 2019;40(14): 4192-4201.
43. Rub U, Hentschel M, Stratmann K, *et al.* Huntington's disease (HD): Degeneration of select nuclei, widespread occurrence of neuronal nuclear and axonal inclusions in the brainstem. *Brain Pathol.* 2014;24(3):247-260.
44. Waldvogel HJ, Kim EH, Tippett LJ, Vonsattel JP, Faull RL. The neuropathology of Huntington's disease. *Curr Top Behav Neurosci.* 2015;22:33-80.
45. Sepers MD, Raymond LA. Mechanisms of synaptic dysfunction and excitotoxicity in Huntington's disease. *Drug Discov Today.* 2014; 19(7):990-996.
46. Heng MY, Detloff PJ, Wang PL, Tsien JZ, Albin RL. In vivo evidence for NMDA receptor-mediated excitotoxicity in a murine genetic model of Huntington disease. *J Neurosci.* 2009;29(10): 3200-3205.
47. Eid L, Parent M. Chemical anatomy of pallidal afferents in primates. *Brain Struct Funct.* 2016;221(9):4291-4317.
48. Oorschot DE. Total number of neurons in the neostriatal, pallidal, subthalamic, and substantia nigral nuclei of the rat basal ganglia: A stereological study using the cavalieri and optical disector methods. *J Comp Neurol.* 1996;366(4):580-599.
49. Reiner A, Dragatsis I, Dietrich P. Genetics and neuropathology of Huntington's disease. *Int Rev Neurobiol.* 2011;98:325-372.
50. Gregory S, Johnson E, Byrne LM, *et al.* Characterizing white matter in Huntington's disease. *Mov Disord Clin Pract.* 2019;7(1):52-60.
51. Faria AV, Ratnanather JT, Tward DJ, *et al.* Linking white matter and deep gray matter alterations in premanifest Huntington disease. *Neuroimage Clin.* 2016;11:450-460.
52. Reading SA, Yassa MA, Bakker A, *et al.* Regional white matter change in pre-symptomatic Huntington's disease: A diffusion tensor imaging study. *Psychiatry Res.* 2005;140(1):55-62.
53. Tabrizi SJ, Scahill RI, Owen G, *et al.* Predictors of phenotypic progression and disease onset in premanifest and early-stage Huntington's disease in the TRACK-HD study: Analysis of 36-month observational data. *Lancet Neurol.* 2013;12(7):637-664.
54. Paulsen JS, Nopoulos PC, Aylward E, *et al.* Striatal and white matter predictors of estimated diagnosis for Huntington disease. *Brain Res Bull.* 2010;82(3-4):201-207.
55. Prusiner SB, Woerman AL, Mordes DA, *et al.* Evidence for α -synuclein prions causing multiple system atrophy in humans with parkinsonism. *Proc Natl Acad Sci U S A.* 2015;112(38): E5308-E5317.
56. Zeighami Y, Ulla M, Iturria-Medina Y, *et al.* Network structure of brain atrophy in de novo Parkinson's disease. *Elife.* 2015;4:e08440.
57. Stopschinski BE, Diamond MI. The prion model for progression and diversity of neurodegenerative diseases. *Lancet Neurol.* 2017; 16(4):323-332.
58. Davis AA, Leys CEG, Holtzman DM. Intercellular spread of protein aggregates in neurodegenerative disease. *Annu Rev Cell Dev Biol.* 2018;34:545-568.
59. Cicchetti F, Lacroix S, Cisbani G, *et al.* Mutant huntingtin is present in neuronal grafts in Huntington disease patients. *Ann Neurol.* 2014;76(1):31-42.
60. Gosset P, Maxan A, Alpaugh M, *et al.* Evidence for the spread of human-derived mutant huntingtin protein in mice and non-human primates. *Neurobiol Dis.* 2020;141:104941.
61. Lee CYD, Wang N, Shen K, *et al.* Disease-related Huntingtin seeding activities in cerebrospinal fluids of Huntington's disease patients. *Sci Rep.* 2020;10(1):20295.
62. Pecho-Vrieseling E, Rieker C, Fuchs S, *et al.* Transneuronal propagation of mutant huntingtin contributes to non-cell autonomous pathology in neurons. *Nat Neurosci.* 2014;17(8):1064-1072.
63. Masnata M, Cicchetti F. The evidence for the spread and seeding capacities of the mutant Huntingtin protein in in vitro systems and their therapeutic implications. *Front Neurosci.* 2017;11:647.
64. Masnata M, Sciacca G, Maxan A, *et al.* Demonstration of prion-like properties of mutant huntingtin fibrils in both in vitro and in vivo paradigms. *Acta Neuropathol.* 2019;137(6):981-1001.
65. Pearce MMP, Kopito RR. Prion-like characteristics of polyglutamine-containing proteins. *Cold Spring Harb Perspect Med.* 2018;8(2):a024257.

66. Virlogeux A, Moutaux E, Christaller W, *et al.* Reconstituting cortico-striatal network on-a-chip reveals the contribution of the presynaptic compartment to Huntington's disease. *Cell Rep.* 2018;22(1):110-122.
67. Saudou F, Humbert S. The biology of huntingtin. *Neuron.* 2016; 89(5):910-926.
68. Lleverenz J, Maher P. Chronic glutamate toxicity in neurodegenerative diseases-what is the evidence? *Front Neurosci.* 2015;9:469.
69. Liddel SA, Guttenplan KA, Clarke LE, *et al.* Neurotoxic reactive astrocytes are induced by activated microglia. *Nature.* 2017; 541(7638):481-487.
70. Hong EP, MacDonald ME, Wheeler VC, *et al.* Huntington's disease pathogenesis: Two sequential components. *J Huntingtons Dis.* 2021;10(1):35-51.
71. Genetic Modifiers of Huntington's Disease Consortium. Electronic address ghmhe, genetic modifiers of huntington's disease C. CAG repeat not polyglutamine length determines timing of huntington's disease onset. *Cell.* 2019;178(4):887-900 e814.
72. Mouro Pinto R, Arning L, Giordano JV, *et al.* Patterns of CAG repeat instability in the central nervous system and periphery in Huntington's disease and in spinocerebellar ataxia type 1. *Hum Mol Genet.* 2020;29(15):2551-2567.
73. Surmeier DJ, Obeso JA, Halliday GM. Parkinson's disease is not simply a prion disorder. *J Neurosci.* 2017;37(41):9799-9807.
74. Fusilli C, Migliore S, Mazza T, *et al.* Biological and clinical manifestations of juvenile Huntington's disease: A retrospective analysis. *Lancet Neurol.* 2018;17(11):986-993.